


ORIGINAL ARTICLE

Open Access



# Accuracy and precision of volumetric bone mineral density assessment using dual-source dual-energy *versus* quantitative CT: a phantom study

Vitali Koch<sup>1</sup>, Nils Große Hokamp<sup>2</sup>, Moritz H. Albrecht<sup>1\*</sup> , Leon D. Gruenewald<sup>1</sup>, Ibrahim Yel<sup>1</sup>, Jan Borggrefe<sup>3</sup>, Stefan Wesarg<sup>4</sup>, Katrin Eichler<sup>5</sup>, Iris Burck<sup>5</sup>, Tatjana Gruber-Rouh<sup>5</sup>, Lukas Lenga<sup>1</sup>, Thomas J. Vogl<sup>1,5</sup>, Simon S. Martin<sup>1</sup>, Julian L. Wichmann<sup>1</sup>, Renate M. Hammerstingl<sup>5</sup>, Leona S. Alizadeh<sup>1</sup>, Christoph Mader<sup>5</sup>, Nicole A. Huizinga<sup>6</sup>, Tommaso D'Angelo<sup>7</sup>, Giorgio Ascenti<sup>7</sup>, Silvio Mazziotti<sup>7</sup> and Christian Booz<sup>1</sup>

## Abstract

**Background:** Dual-source dual-energy computed tomography (DECT) offers the potential for opportunistic osteoporosis screening by enabling phantomless bone mineral density (BMD) quantification. This study sought to assess the accuracy and precision of volumetric BMD measurement using dual-source DECT in comparison to quantitative CT (QCT).

**Methods:** A validated spine phantom consisting of three lumbar vertebra equivalents with 50 (L1), 100 (L2), and 200 mg/cm<sup>3</sup> (L3) calcium hydroxyapatite (HA) concentrations was scanned employing third-generation dual-source DECT and QCT. While BMD assessment based on QCT required an additional standardised bone density calibration phantom, the DECT technique operated by using a dedicated postprocessing software based on material decomposition without requiring calibration phantoms. Accuracy and precision of both modalities were compared by calculating measurement errors. In addition, correlation and agreement analyses were performed using Pearson correlation, linear regression, and Bland-Altman plots.

**Results:** DECT-derived BMD values differed significantly from those obtained by QCT ( $p < 0.001$ ) and were found to be closer to true HA concentrations. Relative measurement errors were significantly smaller for DECT in comparison to QCT (L1, 0.94% *versus* 9.68%; L2, 0.28% *versus* 5.74%; L3, 0.24% *versus* 3.67%, respectively). DECT demonstrated better BMD measurement repeatability compared to QCT (coefficient of variance  $< 4.29\%$  for DECT,  $< 6.74\%$  for QCT). Both methods correlated well to each other ( $r = 0.9993$ ; 95% confidence interval 0.9984–0.9997;  $p < 0.001$ ) and revealed substantial agreement in Bland-Altman plots.

**Conclusions:** Phantomless dual-source DECT-based BMD assessment of lumbar vertebra equivalents using material decomposition showed higher diagnostic accuracy compared to QCT.

**Keywords:** Bone density, Dual-energy computed tomography, Osteoporosis, Phantoms (imaging), Tomography (x-ray computed)

\* Correspondence: [Moritz.Albrecht@kgu.de](mailto:Moritz.Albrecht@kgu.de)

<sup>1</sup>Division of Experimental Imaging, Department of Diagnostic and Interventional Radiology, University Hospital Frankfurt, Theodor-Stern-Kai 7, 60590 Frankfurt am Main, Germany  
Full list of author information is available at the end of the article

## Key points

- Dual-source dual-energy CT (DECT) allowed for accurate bone mineral density (BMD) assessment.
- DECT-based BMD measurements showed a better repeatability in comparison to quantitative CT.
- DECT enables viable retrospective volumetric BMD measurements without requiring calibration phantoms.

## Background

Osteoporosis represents the most common metabolic bone disease characterised by decreased bone mineral density (BMD) and elevated fracture risk [1, 2]. Demographic changes with concomitant increase in osteoporosis entail substantial socio-economic burden [1].

According to the World Health Organization, dual-energy x-ray absorptiometry (DXA) is the current gold standard for BMD assessment due to widespread availability and cost-effectiveness [3]. However, numerous limitations of DXA have been reported, such as the inability to differentiate between cortical and trabecular bone and distortion of BMD measurement through overlying structures [4–8]. Quantitative computed tomography (QCT), the current clinical standard for volumetric BMD assessment, is limitedly available due to high radiation exposure and the need for in-scan calibration using phantoms that do not represent the true composition of trabecular bone and prevent retrospective opportunistic BMD assessment in routinely performed computed tomography (CT) scans [9–11].

Given the increasing number of CT scans in recent years, retrospective BMD assessment by measurement of trabecular Hounsfield units (HU) has been repeatedly suggested, despite being associated with inaccuracies due to inhomogeneous trabecular bone composition as well as technical aspects such as variation of tube voltages [12–15].

Dual-energy CT (DECT) allows for improved material differentiation by using energy dependence of the photoelectric effect at different x-ray spectra [16]. This technique has provided novel and clinically relevant information regarding various musculoskeletal applications compared to conventional CT [17, 18]. Previously, a phantomless dual-source DECT postprocessing algorithm which enables volumetric opportunistic BMD assessment of lumbar trabecular bone by application of dedicated material decomposition has been reported [16]. Initial studies have shown promising results both *in vivo* compared with DXA and *in vitro* compared with pull-out-forces in human cadaver vertebra specimens [19, 20]. In addition, this algorithm yielded significantly

more accurate BMD assessment of the lumbar spine and superior diagnostic accuracy for the detection of osteoporosis compared to HU measurements in a recently published study [21]. However, the accuracy and precision of dual-source DECT has not yet been compared to QCT [22].

We hypothesised that volumetric dual-source DECT using material decomposition may yield more accurate and precise volumetric BMD assessment compared to QCT and facilitates osteoporosis screening by enabling retrospective opportunistic BMD measurements in routine CT scans without the need for calibration phantoms. Thus, the purpose of this study was to compare the accuracy and precision of phantomless dual-source DECT and QCT for volumetric BMD assessment in a prospective phantom study.

## Methods

This prospective phantom study did not need any approval by the institutional review board.

### Phantoms

A standardised anthropomorphic spine phantom (European spine phantom (ESP), serial number ESP-040; QRM GmbH, Moehrendorf, Germany) was used in this study (Fig. 1). The ESP represents a tool for standard quality control in DXA and QCT and contains three different hydroxyapatite (HA) inserts simulating trabecular bone densities of 50.0 (HA 50, L1), 98.4 (HA 100, L2), and 197.6 (HA 200, L3) mg/cm<sup>3</sup> (Fig. 2). It should be noted that the exact HA densities as specified by the

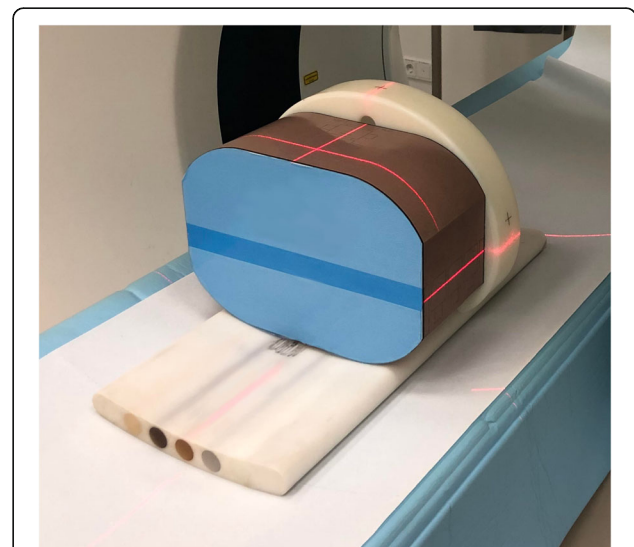
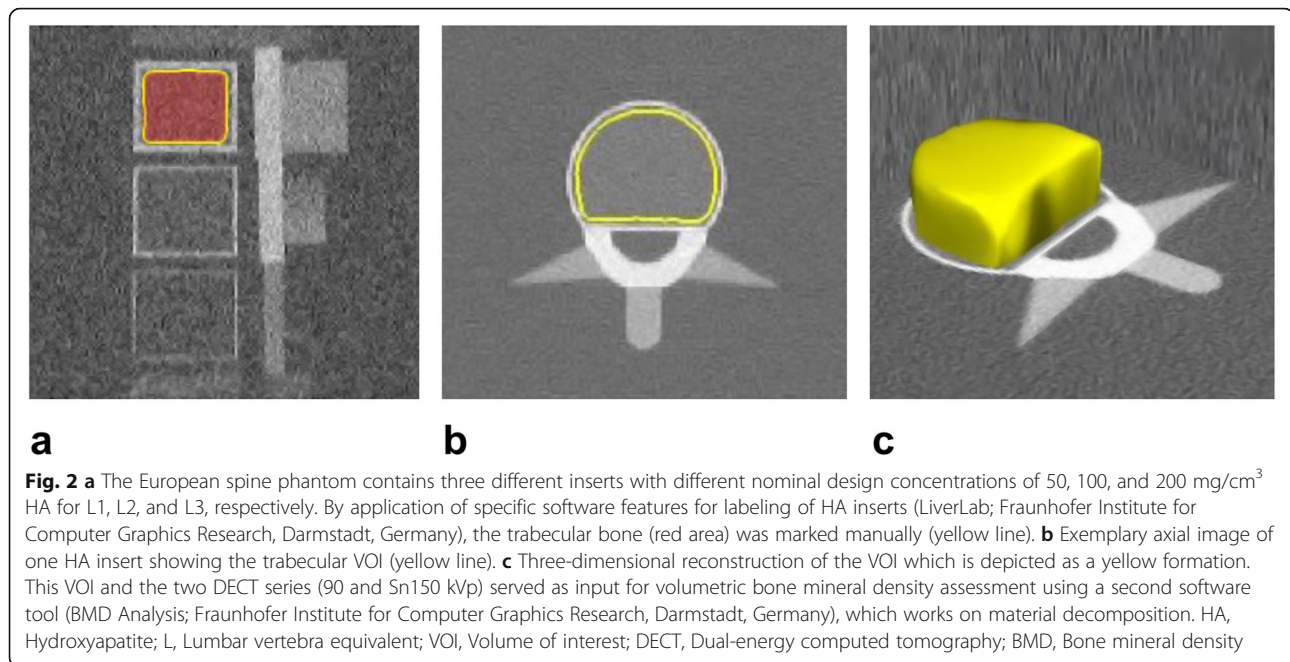


**Fig. 1** Illustration of the European spine phantom (blue, brown) (ESP-040; QRM GmbH, Moehrendorf, Germany) and the QCT bone density calibration phantom (white, below) (BDC-03-29; QRM GmbH, Moehrendorf, Germany). Labels of the manufacturers have been removed. QCT, Quantitative computed tomography



manufacturer were used for the statistical analysis, whereas the nominal values were used only for illustrational purposes in tables and figures.

For QCT calibration, a standardised QCT bone density calibration phantom (BDC, serial number BDC-03-29; QRM GmbH, Moehrendorf, Germany), which contains six cylindrical HA inserts simulating trabecular bone densities of 0, 104.4, 206.2, 402.3, 601.2, and 802.8 mg/cm<sup>3</sup>, was scanned together with the ESP according to clinical standard [7]. For the sake of simplicity, measurement of HA densities in both phantoms is termed BMD measurement in the remaining text. Radiation doses of each scan were noted.

#### Scan protocols and image reconstruction

Scans were generated in craniocaudal direction from L1 to L3 using a third-generation dual-source DECT scanner (Somatom Force; Siemens Healthineers, Forchheim, Germany).

For QCT-based BMD measurements, the ESP and BDC phantom were examined together ten times applying the same QCT scan protocol in each scan. Images were acquired at 120 kVp and 180 mAs using an image section thickness of 1.25 mm according to our standard procedure in clinical routine [23].

For dual-source DECT-based BMD measurements, the ESP was scanned ten times using the same scan protocol as applied in our daily routine for lumbar spine imaging. The two x-ray tubes were operated at different kilovoltage settings (tube A, 90 kVp at 180 mAs; tube B, Sn150 kVp, 0.64 mm tin filter, at 180 mAs) using automatic

attenuation-based tube current modulation (CARE dose 4D; Siemens Healthineers). Three image sets were created from each DECT examination: 90 kVp, Sn150 kVp, and weighted average (ratio, 0.5:0.5) for assimilating contrast properties of single-energy 120 kVp images. For volumetric BMD assessment, image series were reconstructed in axial, coronal, and sagittal planes (section thickness 0.6 mm, increment 0.6 mm) using a dual-energy bone kernel (Br69f).

DECT and QCT images were automatically transferred to the picture archiving and communication system (General Electric Healthcare GmbH, Solingen, Germany).

#### Volumetric BMD assessment

QCT-derived BMD assessment was conducted according to clinical standard using a dedicated workstation and QCT software package (Mindways Software Inc., Austin, USA). Following calibration phantom scanning by using the same protocol as with ESP, the acquired calibration data was stored and used in all subsequent ESP scans for conversion of CT data into BMD values.

Phantomless DECT-based volumetric BMD assessment of L1-3 was based on material decomposition. The trabecular volume of interest (VOI) for each HA insert was manually defined by one reader (M.H.A., radiology resident with 3 years of experience in musculoskeletal imaging) using specific features of the LiverLab software package for labeling of HA inserts (LiverLab; Fraunhofer Institute for Computer Graphics Research, Darmstadt, Germany). The reader was able to determine the VOI in 3D image data sets

which were generated with the uploaded DECT series and if necessary, manually modified for optimal delineation of the trabecular bone.

The obtained data of VOI and the two DECT series (90 and Sn150 kVp) were used for volumetric BMD assessment [16], which was conducted with a second software tool (BMD Analysis; Fraunhofer Institute for Computer Graphics Research) on the basis of material decomposition for each voxel, as initially described by Nickoloff et al. [10] and applied by Wichmann et al. [19]. The previously reported algorithm for material decomposition is based on a biophysical model accounting for the five major substances of trabecular bone (bone minerals, collagen matrix, water, red marrow, and adipose tissue) [21]. Using this model, the following two equations are derived:

$$X^{90}HU = (\mu^{90} - \gamma^{90}g) \cdot V_{TB} + (\beta^{90}t - \gamma^{90}g) \cdot V_F + \gamma^{90}g + \delta \quad (1)$$

$$X^{150}HU = (\mu^{150} - \gamma^{150}g) \cdot V_{TB} + (\beta^{150}t - \gamma^{150}g) \cdot V_F + \gamma^{150}g + \delta \quad (2)$$

These equations link the intensities  $X^{90}$  and  $X^{150}$  (given in HU) in the two CT series obtained at tube energies of 90 and 150 kV to the fraction of the volume occupied by the matrix material (bone mineral + collagen)  $V_{TB}$  and the volume of adipose tissue  $V_F$ . The values for  $t$  and  $g$  are 0.92 g/cm<sup>3</sup> and 1.02 g/cm<sup>3</sup>, respectively, whereas the other variables are energy related constants [10]. By calculating the mean intensity for the trabecular bone in both CT data sets, values for  $V_{TB}$  and  $V_F$  can be attained. Finally, the BMD value  $\rho_{BM}$  (given in g/cm<sup>3</sup>) can be calculated from  $V_{TB}$  by application of the material constants  $l = 3.06$  g/cm<sup>3</sup> and  $\lambda = 2.11$ :

$$\rho_{BM} = \frac{l \cdot V_{TB}}{1 + \lambda} \quad (3)$$

For assessment of spatial BMD distribution, a specific BMD value for each voxel was obtained.

### Statistical analysis

Statistical analysis was performed using commercially available software (MedCalc for Windows, Version 13, MedCalc, Mariakerke, Belgium). Normality of data was tested using the Shapiro-Wilk test. Variables were illustrated as mean  $\pm$  standard deviation. A  $p$  value of less than 0.05 indicated a statistically significant difference.

Accuracy of DECT and QCT for volumetric BMD assessment were assessed by calculating measurement errors for each HA insert. Measurement errors were defined as the difference between the measured BMD and

the true BMD concentration for each HA insert as given by the manufacturer:

$$\text{Measurement error} \left( \frac{\text{mg}}{\text{cm}^3} \right) = \text{Measured BMD} - \text{True BMD}$$

$$\text{Relative measurement error (\%)} = \frac{\text{Measurement error}}{\text{True BMD}} \times 100$$

In addition, the one-sample  $t$  test was used to analyse both BMD assessment approaches with the true BMD values. Furthermore, the paired  $t$  test was used to compare values for L1, L2, and L3 on DECT and QCT. Repeatability as a parameter for precision was assessed by calculating the coefficient of variance. Correlation analysis between DECT and QCT, and between each method and the true BMD was performed by calculating Pearson product-moment correlation ( $r$ ) and linear regression. An  $r$  value of less than 0.4, 0.41–0.6, 0.61–0.8, and greater than 0.8 was considered as poor, moderate, strong, and very strong, respectively. Bland-Altman plots were used to evaluate the agreement of both methods and the agreement of each method with the true BMD value.

### Results

Dual-source DECT-based BMD values for L1 (50 mg/cm<sup>3</sup>), L2 (100 mg/cm<sup>3</sup>), and L3 (200 mg/cm<sup>3</sup>) were 50.47  $\pm$  2.17 mg/cm<sup>3</sup> (mean  $\pm$  standard deviation), 99.72  $\pm$  1.84 mg/cm<sup>3</sup>, and 200.48  $\pm$  2.24 mg/cm<sup>3</sup>, respectively; QCT-derived mean BMD values were 45.16  $\pm$  3.04 mg/cm<sup>3</sup>, 94.26  $\pm$  2.00 mg/cm<sup>3</sup>, and 192.66  $\pm$  2.02 mg/cm<sup>3</sup>, respectively (Table 1). All data from DECT- and QCT-derived BMD measurements were normally distributed ( $p \geq 0.177$ ). Statistical comparison resulted in significant differences between DECT and QCT for L1, L2, and L3 (all  $p < 0.001$ ) (Fig. 3). Overall mean BMD values of L1–L3 inserts were 116.89  $\pm$  63.53 mg/cm<sup>3</sup> (range, 47.10–203.30 mg/cm<sup>3</sup>) for DECT, and 110.69  $\pm$  62.42 mg/cm<sup>3</sup> (range, 41.10–195.30 mg/cm<sup>3</sup>) for QCT ( $p < 0.001$ ). Comparisons of measured BMD values of L1, L2, and L3 with the corresponding true BMD values showed significantly lower BMD results using QCT (all  $p < 0.001$ ), whereas DECT-derived BMD values did not differ significantly when compared to true BMD values (all  $p \geq 0.509$ ) (Fig. 4).

The absolute measurement errors using DECT for the L1, L2, and L3 inserts were 0.47 mg/cm<sup>3</sup>, 0.28 mg/cm<sup>3</sup>, and 0.48 mg/cm<sup>3</sup>, respectively, and 4.84 mg/cm<sup>3</sup>, 5.74 mg/cm<sup>3</sup>, and 7.34 mg/cm<sup>3</sup> using QCT. Relative measurement errors for the L1, L2, and L3 inserts were 0.94%, 0.28%, and 0.24% (DECT), respectively, and 9.68%, 5.74%, and 3.67% using QCT (Table 1).

Repeatability of DECT-derived BMD measurements was better as compared to QCT. Coefficients of variance for the L1, L2, and L3 inserts were 4.29%, 1.85%, and

**Table 1** Values of bone mineral density using dual-source DECT and QCT

Scan	L1 (50 mg/cm <sup>3</sup> )		L2 (100 mg/cm <sup>3</sup> )		L3 (200 mg/cm <sup>3</sup> )	
	DECT	QCT	DECT	QCT	DECT	QCT
1	49.6	42.7	100.8	92.0	197.3	189.7
2	51.1	43.6	98.3	93.2	203.2	191.4
3	50.8	44.2	97.2	91.2	202.2	190.2
4	53.2	45.3	101.2	94.5	198.2	191.8
5	48.8	44.2	102.2	93.9	199.9	193.4
6	47.1	46.2	101.3	95.8	202.3	194.6
7	50.9	51.2	99.4	95.7	203.3	195.3
8	54.2	49.3	98.3	92.7	198.1	191.4
9	48.2	41.1	97.3	96.3	199.2	193.9
10	50.8	43.8	101.2	97.3	201.1	194.9
Mean ± standard deviation	50.47 ± 2.17	45.16 ± 3.04 *	99.72 ± 1.84	94.26 ± 2.00 *	200.48 ± 2.24	192.66 ± 2.02 *
Relative measurement error (%)	0.94	9.68	0.28	5.74	0.24	3.67
Absolute measurement error	0.47	4.84	0.28	5.74	0.48	7.34

Measured BMD values for L1 (50 mg/cm<sup>3</sup>), L2 (100 mg/cm<sup>3</sup>), and L3 (200 mg/cm<sup>3</sup>) using dual-source DECT and QCT imaging. DECT-derived BMD values were closer to true HA concentrations and differed significantly from those obtained by QCT in L1 ( $p < 0.001$ ), L2 ( $p < 0.001$ ), and L3 ( $p < 0.001$ )

\* $p < 0.001$

BMD Bone mineral density, L Lumbar vertebra equivalent, DECT Dual-energy computed tomography, QCT Quantitative computed tomography, HA Hydroxyapatite

1.11% (DECT), respectively, and 6.74%, 2.12%, and 1.05% using QCT.

Mean BMD assessment time for DECT including all postprocessing steps was 4 min (range, 2–6 min), while BMD assessment took 3 min on average for QCT (range, 2–4 min).

### Correlation analysis

Overall correlation analysis showed strong correlation between BMD values derived from DECT and QCT ( $r = 0.9993$ ; 95% CI 0.9984–0.9997;  $p < 0.001$ ). The corresponding Bland-Altman plot demonstrated substantial agreement between DECT and QCT (Fig. 5). Overall DECT-derived BMD values revealed a mean

difference from QCT measurements of  $\bar{d} = 6.20$  mg/cm<sup>3</sup> (95% CI 5.20–7.19 mg/cm<sup>3</sup>;  $p < 0.001$ ), with a standard deviation of 2.67 mg/cm<sup>3</sup>. The 95% limits of agreement were +11.43 mg/cm<sup>3</sup> (95% CI 9.71–13.16 mg/cm<sup>3</sup>) and +0.96 mg/cm<sup>3</sup> (95% CI -0.76–2.68 mg/cm<sup>3</sup>). DECT-derived BMD values for L1, L2, and L3 showed a mean difference from QCT of  $\bar{d} = 5.31$  mg/cm<sup>3</sup> (95% CI 3.27–7.35 mg/cm<sup>3</sup>;  $p < 0.001$ ),  $\bar{d} = 5.46$  mg/cm<sup>3</sup> (95% CI 3.83–7.09 mg/cm<sup>3</sup>;  $p < 0.001$ ), and  $\bar{d} = 7.82$  mg/cm<sup>3</sup> (95% CI 6.18–9.46 mg/cm<sup>3</sup>;  $p < 0.001$ ), respectively.

Furthermore, DECT- and QCT-derived BMD values were highly correlated to true BMD values ( $r = 0.9995$ , 95% CI 0.9989–0.9998 for DECT and  $r = 0.9993$ , 95% CI

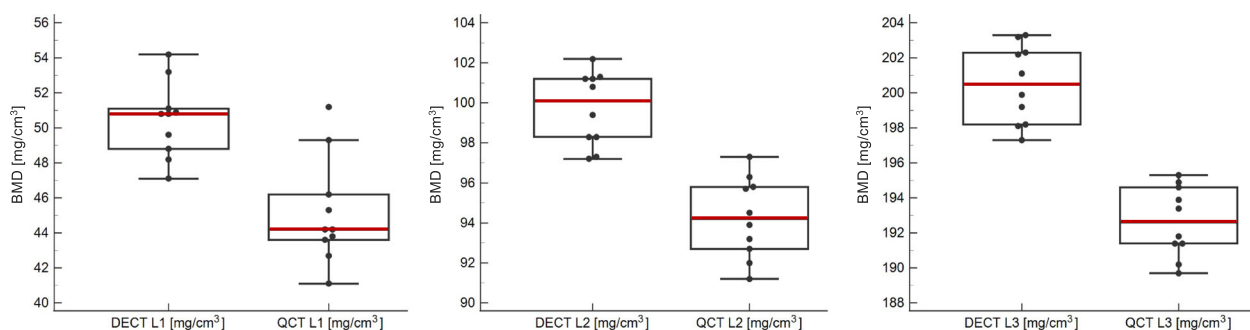
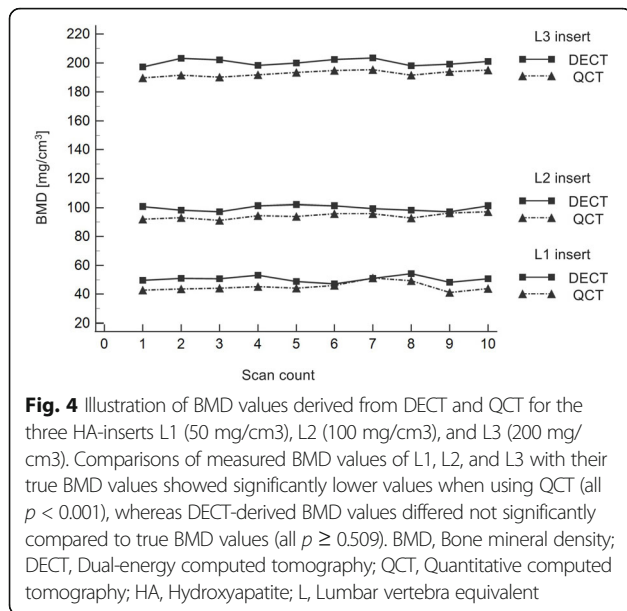


**Fig. 3** Box and whisker plots show DECT-based mean BMD values for L1 (50 mg/cm<sup>3</sup>), L2 (100 mg/cm<sup>3</sup>), and L3 (200 mg/cm<sup>3</sup>) of 50.47 ± 2.17 mg/cm<sup>3</sup>, 99.72 ± 1.84 mg/cm<sup>3</sup>, and 200.48 ± 2.24 mg/cm<sup>3</sup>, respectively; QCT-derived mean BMD values were 45.16 ± 3.04 mg/cm<sup>3</sup>, 94.26 ± 2.00 mg/cm<sup>3</sup>, and 192.66 ± 2.02 mg/cm<sup>3</sup>, respectively. The red line illustrates the mean and the black box edges represent the 25th and 75th percentiles. Statistical comparison resulted in significant differences between DECT and QCT for L1, L2, and L3 (all  $p < 0.001$ ). DECT, Dual-energy computed tomography; BMD, Bone mineral density; L, Lumbar vertebra equivalent; QCT, Quantitative computed tomography



0.9985–0.9997 for QCT, respectively;  $p < 0.001$ ) without significant difference between the two correlation coefficients ( $p = 0.536$ ).

Linear regression analysis was performed on DECT- and QCT-based BMD values for scaling of values and reduction of deviations. For DECT, the regression equation was  $y = 0.0312 + 0.998x$  with  $R^2 = 0.9990$  (Fig. 6a). Using this equation, BMD values for L1, L2, and L3 were scaled to  $50.40 \pm 2.16$  mg/cm<sup>3</sup>,  $99.55 \pm 1.84$  mg/cm<sup>3</sup>, and  $200.11 \pm 2.23$  mg/cm<sup>3</sup>, respectively. The relative measurement errors were adjusted to 0.80%, 0.45%, and 0.06%, respectively.

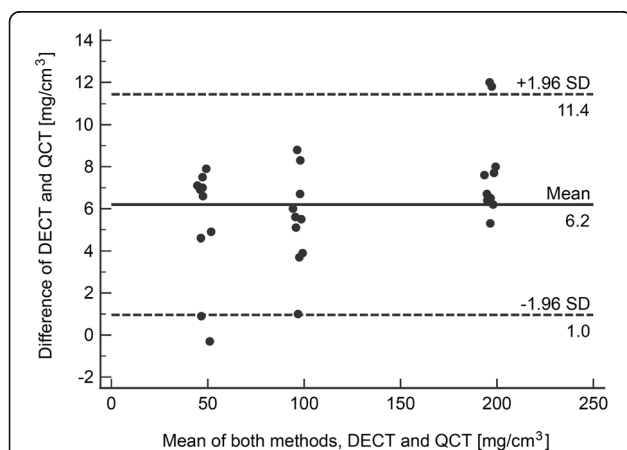
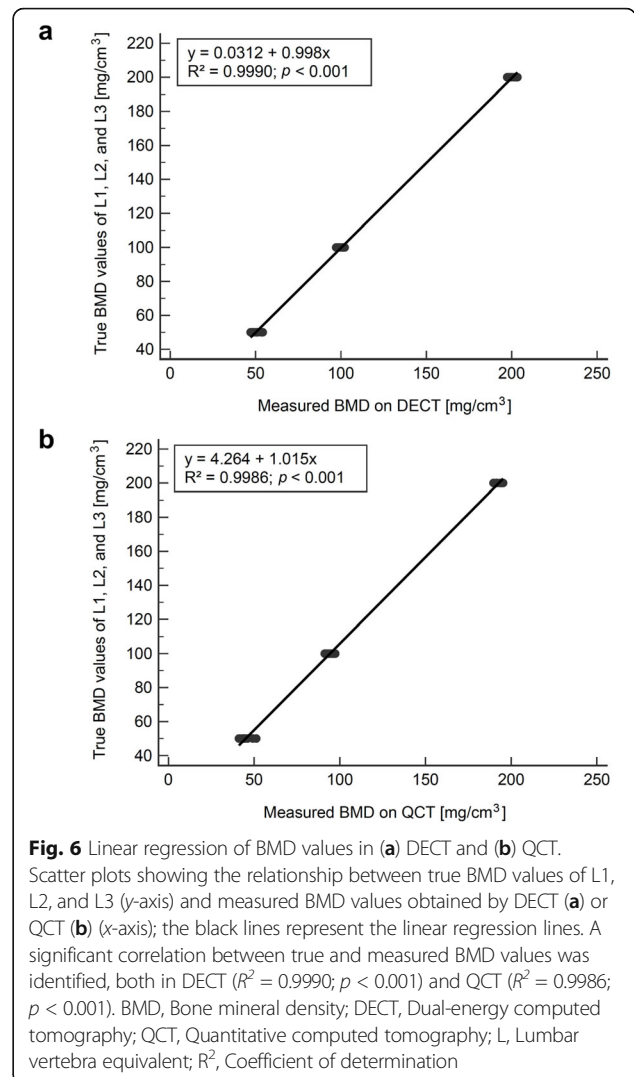


**Fig. 5** Bland-Altman plot illustrating the agreement between dual-source DECT- and QCT-based BMD measurements comprising L1 (50 mg/cm<sup>3</sup>), L2 (100 mg/cm<sup>3</sup>), and L3 (200 mg/cm<sup>3</sup>). Solid line: mean BMD difference. Dot line: 95% limits of agreement (mean difference  $\pm 1.96$  standard deviation). DECT, Dual-energy computed tomography; QCT, Quantitative computed tomography; BMD, Bone mineral density; L, Lumbar vertebra equivalent



For QCT, the regression equation was  $y = 4.264 + 1.015x$  with  $R^2 = 0.9986$  (Fig. 6b). Applying this equation, BMD values for L1, L2, and L3 were scaled to  $50.10 \pm 3.07$  mg/cm<sup>3</sup>,  $99.94 \pm 2.03$  mg/cm<sup>3</sup>, and  $199.81 \pm 2.04$  mg/cm<sup>3</sup>, respectively. The relative measurement errors were reduced to 0.20%, 0.06%, and 0.10%, respectively.

**Radiation dose**

The values of CTDI<sub>vol</sub> values comprising the ten CT scans were  $9.89 \pm 0.33$  mGy (mean  $\pm$  standard deviation) (range, 9.50–10.40 mGy) and  $12.41 \pm 0.27$  mGy (range, 11.90–12.70 mGy) for DECT and QCT ( $p < 0.001$ ), respectively. Mean dose-length product (DLP) values were  $198.54 \pm 6.82$  mGy  $\times$  cm (range, 190.40–209.10 mGy  $\times$  cm) for DECT and  $219.18 \pm 8.69$  mGy  $\times$  cm (range, 205.60–234.80 mGy  $\times$  cm) for QCT ( $p < 0.001$ ) (Table 2).

**Table 2** Radiation doses

	CTDI <sub>vol</sub> (mGy)	DLP (mGy × cm)	kVp	mAs
DECT	9.89 ± 0.33	198.54 ± 6.82	Tube A, 90; tube B, Sn150	180
QCT	12.41 ± 0.27	219.18 ± 8.69	120	180

Mean CTDI<sub>vol</sub> and DLP values differed significantly between DECT and QCT ( $p < 0.001$ ). Data are given as mean ± standard deviation  
CTDI<sub>vol</sub> Volumetric CT dose index, DLP Dose length product, DECT Dual-energy computed tomography, QCT Quantitative computed tomography

## Discussion

Our study showed that phantomless volumetric dual-source DECT-based BMD assessment performed on a spine phantom with three different known HA concentrations yields higher accuracy and precision in comparison to QCT, the current clinical standard for volumetric BMD assessment. In this context, DECT-derived BMD measurements showed a maximal relative measurement error of 0.94% in comparison to 9.68% (QCT). Repeatability of BMD measurement was better using DECT as compared to QCT (coefficient of variance for DECT < 4.29% and for QCT < 6.74%). DECT-derived spine phantom measurements demonstrated high agreement and correlation with QCT ( $r = 0.9993$ ; 95% CI 0.9984–0.9997;  $p < 0.001$ ). The mean BMD assessment time using DECT was 4 min indicating time-efficient applicability in clinical routine.

Opportunistic assessment of BMD has increasingly attracted scientific attention along with demographic changes and the growing prevalence of osteoporosis among older adults [1, 2]. Considering the fact that more than 80 million CT scans are performed each year in the USA [24], patients may highly profit from accurate and precise automated BMD measurements which can be easily derived from routine CT examinations, resulting in lowered costs, resources, radiation exposure, and in a more time-efficient clinical workflow [25]. In this context, application of HU measurements for BMD assessment have been proposed [14, 15, 26], despite being associated with known inaccuracies. Based on the contribution of photoelectric and Compton interactions, bone attenuation values are profoundly affected by tube voltage levels, and the inhomogeneity of trabecular bone composition further influences HU measurements [13, 27]. In addition, the wide range of different devices and manufacturers as well as the applied technique might also affect BMD assessment based on HU measurements.

Nickoloff et al. [10] developed a dedicated material decomposition model based on DECT which facilitates phantomless volumetric opportunistic BMD assessment of trabecular bone. Based on this model, a dual-source DECT postprocessing algorithm for volumetric phantomless BMD assessment of the lumbar spine was

introduced [16]. Wichmann et al. [19] demonstrated the feasibility of this approach in clinical routine, and further evaluated cancellous DECT-based BMD assessment of thoracic and lumbar pedicles in a cadaver study [20]. In addition, a recently published study has shown that phantomless volumetric BMD assessment based on dual-source DECT yields superior diagnostic accuracy for the detection of osteoporosis compared to HU measurements [21]. However, to the best of our knowledge, no prior study has compared dual-source DECT and QCT for volumetric BMD assessment of lumbar vertebrae with regards to accuracy and precision.

Available DECT techniques include dual-source, rapid kilovoltage switching, and dual-layer spectral technologies [28–30]. Dual-source DECT and rapid kilovoltage switching DECT represent the current market leading technologies [28]. Li et al. demonstrated in a recently published phantom study that BMD can be accurately measured either by using DECT or QCT with even smaller bias using DECT compared to QCT [31]. Relative measurement errors of the three different HA inserts were comparable to our study, both in DECT and QCT. The DECT method for BMD assessment was based on rapid kilovoltage switching (Revolution CT, GE, Waukesha, WI, USA) using a different material decomposition algorithm and postprocessing software compared to dual-source DECT. The published phantom study results based on rapid kilovoltage switching were recently reproduced *in vivo* [32]. BMD quantification of the lumbar spine from in total 128 consecutive patients showed a strong correlation and agreement between DECT- and QCT-derived BMD measurements ( $R^2 = 0.983$ – $0.987$ ). However, it should be noted that the applied technique of rapid kilovoltage switching suffers from known limitations regarding modulation and filtration of tube current which can affect BMD measurements, and acquisition times are longer when compared to dual-source DECT [28]. The dual-layer detector technique operates by application of a superficial and a deep layer. Known limitations of this technology include relatively high radiation dose and reduced soft tissue contrast preventing its widespread clinical use in comparison to dual-source DECT [28]. Nevertheless, there have been several studies evaluating the accuracy of dual-layer spectral CT for BMD assessment. In this context, Hamersvelt et al. [33] demonstrated the possibility of accurate BMD quantification using dual-layer spectral CT with strong linear correlations ( $R^2 \geq 0.970$ ;  $p < 0.001$ ) to DXA. Additionally, Roski et al. [34] found high correlations between BMD values derived from dual-layer spectral CT and those from QCT by analysing 174 vertebrae in 33 patients. Another study on the feasibility of dual-layer CT-derived BMD assessment in vertebral specimens and phantom-calibrated QCT measurements

using different setups with varying degrees of obesity reported high correlation between the two modalities unaffected by the obesity grade [35].

In accordance with the aforementioned studies using fat-free phantoms, our observations demonstrated higher BMD values in almost all CT scans obtained with dual-source DECT in comparison to QCT at simultaneously reduced measurement errors. A possible reason for this discrepancy could be technical features of the new generation of DECT spectral imaging technology who comes along with many advantages resulting in better image quality. However, the underestimation of QCT-derived BMD is well known in the clinical setting and may partly be explained by the fat error which significantly affects density measurements and can potentially result in overdiagnosis of osteoporosis [34, 36]. In this context, QCT is influenced by the variable amount of marrow fat leading to accuracy errors of QCT measurements ranging from 2 to 30% [26, 37, 38]. Reasons for this include the operating principle of the single-energy technique, which can only analyse a volume of two components (for example bone mass and red marrow), not taking marrow fat into consideration [37]. Due to dedicated material decomposition, fat-related inaccuracies of BMD measurement can be minimised and overcome by DECT [39].

Another major limitation of QCT-derived BMD assessment represents the need for calibration phantoms that do not represent the true composition of trabecular bone, eliminating the option for opportunistic BMD assessment in routinely performed CT scans which are increasingly conducted in DECT mode. In contrast, DECT offers retrospective phantomless BMD measurements resulting in greater flexibility in clinical routine, rendering additional DXA and QCT examinations unnecessary and thereby substantially reducing radiation exposure, particularly in young patients, premenopausal women, and patients with chronic diseases undergoing repeated follow-up CT scans [19]. While the radiation dose of DXA is relatively low with an effective dose of 0.013 mSv in adults, protocols using QCT for BMD evaluation report effective doses between 1 and 3 mSv [40]. Radiation dose in our study differed significantly between DECT and QCT ( $p < 0.001$ ). Mean CTDI<sub>vol</sub> values for QCT were similar to the data provided by Li et al., whereas CTDI<sub>vol</sub> values for DECT were lower [31]. In addition, DECT has the potential to reduce metal artifacts and permit BMD assessment surrounding metallic implants in the context of adjacent segment degeneration and an increased risk for postoperative fractures [41]. Finally, dual-source DECT-based retrospective BMD assessment may also influence spinal surgeries. The known potential of this technique to compute segmental BMD assessment and to enable a colour-coded

three-dimensional display of trabecular BMD distribution might improve preoperative planning of spondylosis and ensure placement of the pedicle screw in a vertebral segment with higher stability [42].

This study has certain limitations that need to be addressed. First, we used a phantom setting without considering confounding factors that affect BMD assessment, such as the use of intravenous contrast medium, age, gender, body mass index, presence of metal implants, and the fat fraction within vertebral bone marrow. The influence of these factors on BMD assessment could not be evaluated in our phantom study and should be considered in future *in vivo* research. Second, dual-source DECT was evaluated using a single scan protocol, which represents the standard protocol for CT-based lumbar spine imaging in our department. Thus, results and conclusions are vendor- and protocol-specific. Nevertheless, this setup facilitated systematic evaluation of a routinely performed scan protocol under controlled conditions. Third, the ESP phantom represents a relatively small adult person. It thus remains unclear whether our results and conclusions are transferable to patients with other constitutions. Fourth, the accuracy of our DECT approach on calculating volumetric BMD should be evaluated using other energy spectra. Fifth, only predefined lumbar vertebra equivalents were examined without considering biologic variability of BMD and possible BMD variations throughout the lumbar spine [11, 43]. Finally, results of our phantom study have to be confirmed in future studies on humans, evaluating the reproducibility of BMD measurements.

In conclusion, our phantom study demonstrated that phantomless dual-source DECT-derived material decomposition allows for more accurate volumetric BMD assessment compared to QCT at significantly lower radiation dose. Therefore, opportunistic dual-source DECT-derived BMD assessment may serve as a viable alternative to QCT, avoiding unnecessary radiation exposure.

#### Abbreviations

BMD: Bone mineral density; CI: Confidence interval; CT: Computed tomography; CTDI<sub>vol</sub>: Volumetric CT dose index; DECT: Dual-energy CT; DLP: Dose length product; DXA: Dual-energy x-ray absorptiometry; ESP: European spine phantom; HA: Hydroxyapatite; HU: Hounsfield units; QCT: Quantitative CT; VOI: Volume of interest

#### Authors' contributions

VK, CB, and TJV conceived and planned the experiments. MHA and SM analysed the data. NGH, IY, and LDG carried out the experiments. JB, SW, and KE contributed to preparation of the experiments, as well as the visualisation of figures. TGR, IB, LL, and SSM contributed to the interpretation of the results. JLW, RMH, LSA, and CM helped supervise the project. VK, NAH, TD, and GA wrote the manuscript in consultation with CB who revised the manuscript. All authors read and approved the final manuscript.

#### Funding

The authors state that this work has not received any funding. Open Access funding enabled and organised by Projekt DEAL.



**Availability of data and materials**

All data generated or analysed during this study are included in this published article.

**Declarations****Ethics approval and consent to participate**

This prospective phantom study did not need approval by the institutional review board.

**Consent for publication**

Not applicable.

**Competing interests**

IY received a speaking fee from Siemens Healthineers. JLW received speaking fees from Siemens Healthineers and GE Healthcare and was an employee of Siemens Healthineers. MHA received speaking fees from Siemens Healthineers and Bracco. CB received speaking fees from Siemens Healthineers. MHA, TDA are members of the European Radiology Experimental Editorial Board. They have not taken part in the review or selection process of this article. The other authors have no potential competing interests to disclose.

**Author details**

<sup>1</sup>Division of Experimental Imaging, Department of Diagnostic and Interventional Radiology, University Hospital Frankfurt, Theodor-Stern-Kai 7, 60590 Frankfurt am Main, Germany. <sup>2</sup>Department of Diagnostic and Interventional Radiology, University Hospital Cologne, Cologne, Germany. <sup>3</sup>Department of Radiology, Neuroradiology and Nuclear Medicine, Minden Hospital, University of Kiel, Kiel, Germany. <sup>4</sup>Cognitive Computing and Medical Imaging, Fraunhofer IGD, Darmstadt, Germany. <sup>5</sup>Department of Diagnostic and Interventional Radiology, University Hospital Frankfurt, Frankfurt am Main, Germany. <sup>6</sup>Interdisciplinary Center for Neuroscience, Goethe University of Frankfurt, Frankfurt am Main, Germany. <sup>7</sup>Department of Biomedical Sciences and Morphological and Functional Imaging, University Hospital Messina, Messina, Italy.

Received: 17 June 2021 Accepted: 26 August 2021

Published online: 05 October 2021

**References**

- Burge R, Dawson-Hughes B, Solomon DH, Wong JB, King A, Tosteson A (2007) Incidence and economic burden of osteoporosis-related fractures in the United States, 2005–2025. *J Bone Miner Res* 22:465–475. <https://doi.org/10.1359/jbmr.061113>
- Cummings SR, Kelsey JL, Nevitt MC, O'Dowd KJ (1985) Epidemiology of osteoporosis and osteoporotic fractures. *Epidemiol Rev* 7:178–208. <https://doi.org/10.1093/oxfordjournals.epirev.a036281>
- Kanis DR, Ratner MA, Marks TJ (1994) Design and construction of molecular assemblies with large second-order optical nonlinearities Quantum chemical aspects. *Chem Rev* 94:195–242. <https://doi.org/10.1021/cr00025a007>
- Svendsen OL, Hassager C, Skodt V, Christiansen C (1995) Impact of soft tissue on in vivo accuracy of bone mineral measurements in the spine, hip, and forearm: a human cadaver study. *J Bone Miner Res* 10:868–873. <https://doi.org/10.1002/jbmr.5650100607>
- Antonucci MD, Hanson DS, Heggeness MH (1996) Pitfalls in the measurement of bone mineral density by dual energy x-ray absorptiometry. *Spine (Phila Pa 1976)* 21:87–91. <https://doi.org/10.1097/00007632-199601010-00020>
- Bolotin H (2007) DXA in vivo BMD methodology: an erroneous and misleading research and clinical gauge of bone mineral status, bone fragility, and bone remodelling. *Bone* 41:138–154. <https://doi.org/10.1016/j.bone.2007.02.022>
- Engelke K, Lang T, Khosla S, et al (2015) Clinical use of quantitative computed tomography-based advanced techniques in the management of osteoporosis in adults: the 2015 ISCD Official Positions—Part III. *J Clin Densitom* 18:393–407. <https://doi.org/10.1016/j.jocd.2015.06.010>
- Kwon D, Kim J, Lee H et al (2018) Quantitative computed tomographic evaluation of bone mineral density in beagle dogs: comparison with dual-energy x-ray absorptiometry as a gold standard. *J Vet Med Sci* 80:620–628. <https://doi.org/10.1292/jvms.17-0428>
- Rao GU, Yaghai I, Wist AO, Arora G (1987) Systematic errors in bone-mineral measurements by quantitative computed tomography. *Med Phys* 14:62–69. <https://doi.org/10.1118/1.596096>
- Nickoloff EL, Feldman F, Atherton JV (1988) Bone mineral assessment: new dual-energy CT approach. *Radiology* 168:223–228. <https://doi.org/10.1148/radiology.168.1.3380964>
- Wong M, Papa A, Lang T, Hodis HN, Labree L, Detrano R (2005) Validation of thoracic quantitative computed tomography as a method to measure bone mineral density. *Calcif Tissue Int* 76:7–10. <https://doi.org/10.1007/s00223-004-0020-5>
- Lee S, Binkley N, Lubner M, Bruce R, Ziemlewicz T, Pickhardt P (2016) Opportunistic screening for osteoporosis using the sagittal reconstruction from routine abdominal CT for combined assessment of vertebral fractures and density. *Osteoporosis Int* 27:1131–1136. <https://doi.org/10.1007/s00198-015-3318-4>
- Garner HW, Paturzo MM, Gaudier G, Pickhardt PJ, Wessell DE (2017) Variation in attenuation in L1 trabecular bone at different tube voltages: caution is warranted when screening for osteoporosis with the use of opportunistic CT. *AJR Am J Roentgenol* 208:165–170. <https://doi.org/10.2214/AJR.16.16744>
- Jang S, Graffy PM, Ziemlewicz TJ, Lee SJ, Summers RM, Pickhardt PJ (2019) Opportunistic osteoporosis screening at routine abdominal and thoracic CT: normative L1 trabecular attenuation values in more than 20 000 adults. *Radiology* 291:360–367. <https://doi.org/10.1148/radiol.2019181648>
- Pickhardt PJ, Pooler BD, Lauder T, del Rio AM, Bruce RJ, Binkley N (2013) Opportunistic screening for osteoporosis using abdominal computed tomography scans obtained for other indications. *Ann Intern Med* 158:588–595. <https://doi.org/10.7326/0003-4819-158-8-201304160-00003>
- Wesarg S, Kirschner M, Becker M, Erdt M, Kafchitsas K, Khan M (2012) Dual-energy CT-based assessment of the trabecular bone in vertebrae. *Methods Inf Med* 51:398–405. <https://doi.org/10.3414/ME11-02-0034>
- Petrtsch B, Kosmala A, Weng AM, et al (2017) Vertebral compression fractures: third-generation dual-energy CT for detection of bone marrow edema at visual and quantitative analyses. *Radiology* 284:161–168. <https://doi.org/10.1148/radiol.2017162165>
- Booz C, Noske J, Martin SS et al (2019) Virtual noncalcium dual-energy CT: detection of lumbar disk herniation in comparison with standard gray-scale CT. *Radiology* 290:446–455. <https://doi.org/10.1148/radiol.2018181286>
- Wichmann JL, Booz C, Wesarg S, et al (2014) Dual-energy CT-based phantomless in vivo three-dimensional bone mineral density assessment of the lumbar spine. *Radiology* 271:778–784. <https://doi.org/10.1148/radiol.13131952>
- Wichmann JL, Booz C, Wesarg S, et al (2015) Quantitative dual-energy CT for phantomless evaluation of cancellous bone mineral density of the vertebral pedicle: correlation with pedicle screw pull-out strength. *Eur Radiol* 25:1714–1720. <https://doi.org/10.1007/s00330-014-3529-7>
- Booz C, Noeske J, Albrecht MH, et al (2020) Diagnostic accuracy of quantitative dual-energy CT-based bone mineral density assessment in comparison to Hounsfield unit measurements using dual x-ray absorptiometry as standard of reference. *Eur J Radiol* 132:109321. <https://doi.org/10.1016/j.ejrad.2020.109321>
- Expert Panel on Musculoskeletal Imaging, Ward RJ, Roberts CC, et al (2017) ACR appropriateness criteria(R) osteoporosis and bone mineral density. *J Am Coll Radiol* 14:189–202. <https://doi.org/10.1016/j.jacr.2017.02.018>
- Brett AD, Brown JK (2015) Quantitative computed tomography and opportunistic bone density screening by dual use of computed tomography scans. *J Orthop Translat* 3:178–184. <https://doi.org/10.1016/j.jot.2015.08.006>
- Murthy A, Kornel E, Neubardt S (2021) Strategy to reduce radiation exposure in postoperative spinal computed tomography scans. *Surg Neurol Int* 12: 159. [https://doi.org/10.25259/SNI\\_289\\_2020](https://doi.org/10.25259/SNI_289_2020)
- Gajawelli N, Tsao S, Kromnick M, Nelson M, Lepore N (2019) Image postprocessing adoption trends in clinical medical imaging. *J Am Coll Radiol* 16:945–951. <https://doi.org/10.1016/j.jacr.2019.01.005>
- Mao SS, Luo Y, Fischer H, Buodff MJ, Li D (2016) Routine coronary calcium scan can precisely measure vertebral bone density without a quantitative calibration phantom. *J Comput Assist Tomogr* 40:126–130. <https://doi.org/10.1097/RCT.00000000000000330>
- Mazess RB (1983) Errors in measuring trabecular bone by computed tomography due to marrow and bone composition. *Calcif Tissue Int* 35: 148–152. <https://doi.org/10.1007/BF02405022>
- Mallinson PI, Coupal TM, McLaughlin PD, Nicolaou S, Munk PL, Ouellette HA (2016) Dual-energy CT for the musculoskeletal system. *Radiology* 281:690–707. <https://doi.org/10.1148/radiol.2016151109>
- Arentsen L, Hansen KE, Yagi M, et al (2017) Use of dual-energy computed tomography to measure skeletal-wide marrow composition and cancellous

- bone mineral density. *J Bone Miner Metab* 35:428–436. <https://doi.org/10.1007/s00774-016-0796-1>
30. Wait JM, Cody D, Jones AK, Rong J, Baladandayuthapani V, Kappadath SC (2015) Performance evaluation of material decomposition with rapid-kilovoltage-switching dual-energy CT and implications for assessing bone mineral density. *AJR Am J Roentgenol* 204:1234–1241. <https://doi.org/10.2214/AJR.14.13093>
  31. Li X, Li X, Li J, et al (2020) The accuracy of bone mineral density measurement using dual-energy spectral CT and quantitative CT: a comparative phantom study. *Clin Radiol* 75:320.e9–320.e15. <https://doi.org/10.1016/j.crad.2019.11.008>
  32. Zhou S, Zhu L, You T et al (2021) In vivo quantification of bone mineral density of lumbar vertebrae using fast kVp switching dual-energy CT: correlation with quantitative computed tomography. *Quant Imaging Med Surg* 11:341–350. <https://doi.org/10.21037/qims-20-367>
  33. van Hamersvelt RW, Schilham AMR, Engelke K, et al (2017) Accuracy of bone mineral density quantification using dual-layer spectral detector CT: a phantom study. *Eur Radiol* 27:4351–4359. <https://doi.org/10.1007/s00330-017-4801-4>
  34. Roski F, Hammel J, Mei K, et al (2019) Bone mineral density measurements derived from dual-layer spectral CT enable opportunistic screening for osteoporosis. *Eur Radiol* 29:6355–6363. <https://doi.org/10.1007/s00330-019-06263-z>
  35. Mei K, Schwaiger BJ, Kopp FK, et al (2017) Bone mineral density measurements in vertebral specimens and phantoms using dual-layer spectral computed tomography. *Sci Rep* 7:17519. <https://doi.org/10.1038/s41598-017-17855-4>
  36. Yu EW, Thomas BJ, Brown JK, Finkelstein JS (2012) Simulated increases in body fat and errors in bone mineral density measurements by DXA and QCT. *J Bone Miner Res* 27:119–124. <https://doi.org/10.1002/jbmr.506>
  37. Kuiper JW, van Kuijk C, Grashuis JL, Ederveen AG, Schutte HE (1996) Accuracy and the influence of marrow fat on quantitative CT and dual-energy x-ray absorptiometry measurements of the femoral neck in vitro. *Osteoporos Int* 6:25–30. <https://doi.org/10.1007/BF01626534>
  38. Malekzadeh M, Abbasi-Rad S, Shahgholi M, et al (2019) Design and validation of synchronous QCT calibration phantom: practical methodology. *J Med Imaging Radiat Sci* 50:157–162. <https://doi.org/10.1016/j.jmir.2018.10.002>
  39. Qin L, Huang J, Yu P, et al (2021) Accuracy, agreement, and reliability of DECT-derived vBMD measurements: an initial ex vivo study. *Eur Radiol* 31: 191–199. <https://doi.org/10.1007/s00330-020-07118-8>
  40. Damilakis J, Adams JE, Guglielmi G, Link TM (2010) Radiation exposure in x-ray-based imaging techniques used in osteoporosis. *Eur Radiol* 20:2707–2714. <https://doi.org/10.1007/s00330-010-1845-0>
  41. Bamberg F, Dierks A, Nikolaou K, Reiser MF, Becker CR, Johnson TR (2011) Metal artifact reduction by dual energy computed tomography using monoenergetic extrapolation. *Eur Radiol* 21:1424–1429. <https://doi.org/10.1007/s00330-011-2062-1>
  42. Nottmeier EW, Pirris SM (2013) Placement of thoracic transvertebral pedicle screws using 3D image guidance: presented at the 2012 Joint Spine Section Meeting. *J Neurosurg Spine* 18:479–483. <https://doi.org/10.3171/2013.2.SPINE12819>
  43. Salzmänn SN, Shirahata T, Yang J, et al (2019) Regional bone mineral density differences measured by quantitative computed tomography: does the standard clinically used L1-L2 average correlate with the entire lumbosacral spine? *Spine J* 19:695–702. <https://doi.org/10.1016/j.spinee.2018.10.007>

## Publisher's Note

Springer Nature remains neutral with regard to jurisdictional claims in published maps and institutional affiliations.

Submit your manuscript to a SpringerOpen<sup>®</sup> journal and benefit from:

- Convenient online submission
- Rigorous peer review
- Open access: articles freely available online
- High visibility within the field
- Retaining the copyright to your article

---

Submit your next manuscript at ► [springeropen.com](https://www.springeropen.com)

---